



HAL
open science

Source Localization of Microseismic Emissions During Pneumatic Fracturing

Antoine L. Turquet, Renaud Toussaint, Fredrik Kvalheim Eriksen, Guillaume Daniel, Olivier Lengliné, Eirik G. Flekkøy, Knut Jørgen Måløy

► **To cite this version:**

Antoine L. Turquet, Renaud Toussaint, Fredrik Kvalheim Eriksen, Guillaume Daniel, Olivier Lengliné, et al.. Source Localization of Microseismic Emissions During Pneumatic Fracturing. *Geophysical Research Letters*, 2019, 46 (7), pp.3726-3733. 10.1029/2019GL082198 . hal-02130588

HAL Id: hal-02130588

<https://hal.science/hal-02130588>

Submitted on 15 May 2019

HAL is a multi-disciplinary open access archive for the deposit and dissemination of scientific research documents, whether they are published or not. The documents may come from teaching and research institutions in France or abroad, or from public or private research centers.

L'archive ouverte pluridisciplinaire **HAL**, est destinée au dépôt et à la diffusion de documents scientifiques de niveau recherche, publiés ou non, émanant des établissements d'enseignement et de recherche français ou étrangers, des laboratoires publics ou privés.

Source Localization of Microseismic Emissions during Pneumatic Fracturing

Antoine L. Turquet^{1*}, Renaud Toussaint^{1,2,3}, Fredrik Kvalheim Eriksen^{1,2}, Guillaume
Daniel⁴, Olivier Lengliné^{1,3}, Eirik G. Flekkøy^{2,3}, Knut Jørgen Måløy^{2,3}

¹University of Strasbourg, Institut de Physique du Globe de Strasbourg, CNRS UMR7516, 5 Rue Descartes, F-67000
Strasbourg, France

²SFF PoreLab, The Njord Centre, Department of Physics, University of Oslo, PO Box 1048, Blindern, N-0316, Oslo,
Norway

³International Associate Laboratory LIA D-FFRACT, Deformation, Flow and Fracture of Disordered Materials,
France-Norway

⁴EDF - Direction Industrielle, Aix-en-Provence, France

Key Points:

- The pneumatic fracturing experiments in a Hele-Shaw cell are monitored using accelerometers and a high speed camera.
- The acoustic emissions are localized using an energy based signal location method and displacement maps are obtained from image correlation.
- By comparing the acoustic and the optical results we observe the motion starts in porous medium and propagates towards the channel tips.

*Currently working at ENS Lyon, France

Abstract

Localization of signals is a widely applied technique used in different areas of science telecommunication, medicine or seismology. In this work, we study microseismic emissions due to stick-slip events during pneumatic fracture in a transparent setup at laboratory scale and apply a localization method "Estimated Source Energy Homogeneity". The seismic location results are compared with the image correlation results for displacement maps corresponding to the event times. We have observed (using optics and acoustics) that the movement starts inside the porous medium and progresses towards the channel tips, eventually causing channels to grow further. This finding could be of interest in understanding fluid-induced earthquake nucleation processes. Similar to in-site applications of pneumatic or fluid-related fracturing, it shows that the area influenced extends beyond the fracture tips. This also shows why even after the end of pumping, we may get earthquakes, such as in the Basel case [Haring et al. 2008].

1 Introduction

Acoustic signal localization is applied in many different areas of science [Gershman et al., 1995; Valin et al., 2003; Elnahrawy et al., 2004; Malioutov et al., 2005; Zhu et al., 2007; Fink, 2015; Garnier and Fink, 2015]. In robotics, speech-source tracking is done to automate cameras to follow the speaker [Brandstein et al., 1997]. In electronics, touchscreens are a very popular example of a signal localization. It is necessary for the system to locate the touch of a user to transmit information to process a simple message [Terlizzi and Mino, 2009].

Similarly, in earth sciences, finding the epicenter of an earthquake is necessary to understand how it was generated, where exactly the movement occurred, which region is more risky for the aftershocks [Aki and Richards, 2002], [Turquet et al., 2018a]. For a better quality risk assessment, it is important to know the origin of the seismicity along with its location. In nature, seismic events based on gas-solid interactions are very common. For example, there are many existing studies about a volcano-heated fluid becomes gas causing phreatic eruptions or geysers [Tazieff, 1989; Oppenheimer, 1986; Manga and Brodsky, 2006; Christenson et al., 2010; Jolly et al., 2014; Sudo et al., 1998]. Moreover, fast air or fluid injection deforming porous medium is used in the industrial applications of pneumatic fracturing [Schuring et al., 1996; Accutech, 1994; Gao et al., 2014] or hydraulic fracturing [Charl ty et al., 2007; Cuenot et al., 2008; Dorbath et al., 2009; Aochi

51 *et al.*, 2011]. At very large scales (tens or hundreds of meters) and high-pressure injec-
52 tion, compressibility plays role in the interactions between the pressurized fluid and de-
53 formable solid medium similar to the gas-solid interactions mentioned earlier. This phys-
54 ical phenomenon can be observed in magma fracturing, eruptions [*Rivalta and Segall*,
55 2007; *Poland et al.*, 2012], fluid injecting into rocks, or reservoir stimulations in geother-
56 mal fields [*Candela et al.*, 2018]. *Stanchits et al.* [2011] have studied the acoustic emis-
57 sions on rock samples during thermo-hydro-chemo-mechanical coupled deformations. Wa-
58 ter injection into porous sandstone under applied stress induced acoustic emission events.
59 These events are generated close to the migrating waterfront. *Kobchenko et al.* [2013]
60 studied the transport of CO₂ by diffusion and fracturing the gel layer in a Hele-Shaw cell.
61 They studied the length scales of diffusion and flow in fracture networks which are eventu-
62 ally linked to statistical properties of river networks and hierarchical-fracture networks. In
63 the very recent research of *Jamtveit et al.* [2018], they have found that the strike-slip lower
64 crust earthquakes are causing fluid pressure pulses towards the lower crust and fluid-driven
65 associated metamorphic and structural transformations of the lower crust follow these
66 earthquakes. More importantly, at large scales, a common way to understand and control
67 the fluid induced fracturing is to monitor the microseismicity [*Holland*, 2013; *Valkó and*
68 *Economides*, 1995; *Cornet et al.*, 1998; *Cornet*, 2015; *Fehler et al.*]. The source locations
69 of seismic events are mainly focusing on the fluid-solid coupled events.

70 Even though the localization of the microseismicity due to volcanoes, and industrial
71 applications such as hydraulic fracturing has a very rich scientific literature, the locations
72 of acoustic emissions based on interactions between the injected gas and deformable the
73 solid (or gas-metal in pressure tanks [*Peacock*, 1996]) remains challenging. To the best
74 of our knowledge, acoustic emissions have not been studied during pneumatic fractures in
75 the scientific literature prior to this article. In this article, we are investigating the source
76 mechanics and locations of pneumatic fractures in a porous medium in a transparent Hele-
77 Shaw cell. The main focus of this work is to first locate the stick-slip events using acous-
78 tic emissions and then to compare them with the displacement field obtained from digital
79 image correlation. The main reason behind using a Hele-Shaw cell is to optically record
80 the deformations associated with the microseismic event while recording the vibrations
81 on the glass plate with accelerometers. This work is based on the similar experiments as
82 in the previous works done by *Turkaya et al.* [2015], *Eriksen et al.* [2017a], *Eriksen et al.*
83 [2018], and *Turquet et al.* [2018b].

84 Recently, some of the signal localization types are reviewed in the work *Turkaya*
 85 *et al.* [2016]. Here in this article, we show the application of Estimation of Source Energy
 86 Homogeneity (ESEH) to locate the source of the acoustic emissions during aerofracturing
 87 experiments [*Turkaya et al.*, 2015]. These localization results are compared with the Dig-
 88 ital Image Correlation (details can be found in *Eriksen et al.* [2017a] results), as obtained
 89 from the optical recordings via a high-speed camera during the experiment.

90 **2 Experimental setup**

91 The aerofracturing experiments analyzed here are conducted in a Hele-Shaw cell
 92 made of two glass plates 80 cm × 40 cm × 1 cm with an aperture of 1 mm between them
 93 - see details in *Turkaya et al.* [2015], *Eriksen et al.* [2017b], *Eriksen et al.* [2018], and
 94 *Turquet et al.* [2018b]. The experimental setup is shown in Figure 1(a). The acquisition
 95 chains of optical and acoustic data are presented. The system is triggered via a signal
 96 generator to have synchronization between optical and acoustic data. The optical data
 97 were recorded at 125 or 1000 images per second using a Photron SA5 and a flicker-free
 98 Dedolight 400W projector, and for acoustic data, we use 1 MHz sampling rate. Three
 99 boundaries of this cell are sealed with a double-sided tape while the fourth side is cov-
 100 ered with a 40 μm mesh filter. This filter lets the air pass to the surrounding atmosphere
 101 while keeping the grains inside of the cell. In this particular experiment, we used 1 bar
 102 overpressure from the inlet and we used 80 μm grains having material density 1.05 g/cm^3
 103 in loose state inside the cell. Prior to the experiment, the cell is filled vertically before
 104 sealing with a semi-permeable mesh. Then, the cell is rotated vertically so that the grains
 105 free fall to the other end of the cell without any external effect. This enables that the solid
 106 ratio is very close to the random loose packing with a solid fraction of $\phi = 0.44 \pm 0.04$
 107 [*Eriksen et al.*, 2017b]. Finally, the cell is carefully placed horizontally without changing
 108 this loose state. This simple preparation procedure ensures that the experiments are repro-
 109 ducible. An empty space is provided between the air inlet and the solid-air interface to
 110 provide a homogenous pressure over the width of the cell. The air overpressure at the inlet
 111 is then raised and maintained at a constant level (1 bar in the example on Figure 1).

119 During this experiment, acoustic signals are recorded using 4 accelerometers at-
 120 tached to the bottom plate (see Figure 1(b)). The sensors are placed towards the outlet
 121 (where most of the stick-slip events are happening) to have a better signal resolution. The
 122 sensors are Miniature piezoelectric charge accelerometer 4374 - Brüel & Kjaer associated

123 to a NEXUS Charge Amplifier - Type 2692-A conditioner, and the signal is digitized us-
 124 ing a National Instruments NI-DAQ mx acquisition card PCI-6133 8 Channels acquisition
 125 card. The accelerometers have 1 Hz to 26 kHz flat response. Using the function given by
 126 the manufacturer the response is flattened up to 200 kHz. These accelerometers can record
 127 only normal direction to the glass plate. Depending on the sign of the cumulative dis-
 128 placement (positive or negative) recorded at the sensor we mark the corresponding signals
 129 with the polarisation up or down respectively. The acoustic events are located using ESEH
 130 for a certain window of the signal which starts at the arrival time and ends somewhere in
 131 the coda. We have presented a more detailed discussion linking the acoustic signal polar-
 132 ization to medium deformation in Supplementary Text S1. More information about time
 133 windowing can be obtained from Supplementary Figure S1 and associated caption. Fur-
 134 thermore, the procedure of detecting the acoustic events from raw recordings is described
 135 in the Supplementary Text S2.

136 3 Estimation of Source Energy Homogeneity (ESEH)

137 Estimation of Source Energy Homogeneity considers that the source energy calcu-
 138 lated from different recordings should be the same after the correction of energy loss due
 139 to the travel-path attenuation (based on material and distance). If we express the source
 140 energy with E_s and consider that the energy spread cylindrically on the plates the recorded
 141 energy E_n at receiver n at a distant R can be expressed with $E_n = \frac{E_s}{2\pi R h}$ where h is the
 142 plate thickness. E_s can be estimated following *Hibert et al.* [2011]; *Farin et al.* [2016];
 143 *Turkaya et al.* [2016] by:

$$E_s(\mathbf{r}_s, \mathbf{r}_n) = \int_0^{\omega_{Nyq}} 2\pi R(n) \rho h c(\omega) \frac{|a(\omega)|^2}{\omega^2} d\omega, \quad (1)$$

144 where $E_s(\mathbf{r}_s, \mathbf{r}_n)$ is the computed energy coming from a source at \mathbf{r}_s recorded by a sensor
 145 at \mathbf{r}_n . ρ is the mass density of the plate, $c(\omega)$ is the group velocity of the waves over dif-
 146 ferent angular frequencies ω up to Nyquist frequency ω_{Nyq} , $a(\omega)$ is the Fourier transform
 147 of the accelerometric recordings. $R(n) = \|\mathbf{r}_n - \mathbf{r}_s\|$ is the distance between the source and
 148 the receiver and h is the plate thickness. Depending on the plate material there could be a
 149 viscous attenuation factor $e^{(2\gamma(\omega)R(n))}$ added to the right side of the Eq. (1) to account for
 150 viscous energy losses where $\gamma(\omega)$ is the viscous attenuation inverse distance. However, for
 151 glass plates and the distances that are used in this experiment viscous attenuation can be
 152 neglected (i.e. $\gamma \approx 0$ [*Farin et al.*, 2015]). In the experimental setup, 4 sensors are placed
 153 on the bottom glass plate on different locations (see Figure 1b and c) to have a good spa-

154 tial coverage. Standard deviation $\sigma(\mathbf{r}_s)$ for source energy E_s at different test positions \mathbf{r}_s
 155 on a regular grid for 4 different sensors are calculated. The minimum of this standard de-
 156 viation indicates over all tested positions \mathbf{r}_s the source location [Turkaya *et al.*, 2016]. We
 157 used 5 mm grid spacing for the trial positions \mathbf{r}_s on the 45 cm \times 30 cm area covered by
 158 the porous medium inside the Hele-Shaw cell.

159 **4 Image processing for deformation localization**

160 The optical images were captured via a high-speed camera (FastCam SA5 - Photron,
 161 recorded with 125 or 1000 fps with a resolution 1024 \times 1024 pixels) during the exper-
 162 iments. These images are investigated to localize the deformation corresponding to the
 163 time interval when the acoustic signal is emitted. The deformation of the medium dur-
 164 ing the acoustic emission is analyzed based on the image analysis techniques eventually
 165 producing frame-to-frame displacement fields of the porous medium [Eriksen *et al.*, 2015,
 166 2017b,a; Niebling *et al.*, 2010; Travelletti *et al.*, 2012; Chevalier *et al.*, 2009].

167 First, two successive images corresponding to the start and the end of the acous-
 168 tic event is taken. Following this pre-treatment, a Digital Image Correlation (DIC) pro-
 169 cedure, called Ncorr (an open source 2D digital image correlation MATLAB software)
 170 is applied to obtain frame-to-frame displacement fields. Ncorr cross-correlates subwin-
 171 dows between two images to find displacement fields in between. A detailed description
 172 of Ncorr is given in Blaber *et al.* [2015].

173 In Figure 2(a), an example of the displacement magnitude field obtained is given
 174 in the background. This map shows the magnitude of the absolute displacement of the
 175 medium (without any defined direction in the format of $||\vec{u}|| = \sqrt{u_x^2 + u_y^2}$ where $u_{x,y}$ are
 176 the displacements in directions x and y) occurring between two images taken at 8 ms from
 177 each other. The colormap shows the norm of the displacement field over the Hele-Shaw
 178 cell. As it can be seen for this snapshot, the displacements are focused on the fingertips.
 179 However, it is still possible to see nonzero displacements (of lower amplitudes) farther
 180 from the fingertips into the porous medium.

181 **5 Results and Discussion**

182 In Figure 2 the localization for an acoustic event is given. Displacement maps (in
 183 grey) are overlaid by acoustic localization results. Markers with different colors are calcu-

184 lated for different time window lengths to define the primary signal (see Supplementary
185 Figure S1 for window lengths). The size of the time window is set to extend stepwise to
186 give multiple estimations for a single event for a better comparison with DIC results. DIC
187 gives us an idea about the evolution of the signal location by indicating the location of the
188 displacement occurred during this time interval. In Figure 2 we see that the event source
189 starts inside the porous medium and progresses towards the channel tips. Moreover, by
190 increasing the size of the time window of the signal, we increase the sensitivity of the
191 sensors for the waves coming from a larger area. The waves propagating on thin plates -
192 similar to the glass plates which are used in this experimental study - may propagate at
193 different velocities as a function of their frequency, which is the definition of dispersive
194 waves. In this work, the "dispersivity" of the Lamb Waves are taken into account in wave
195 velocity calculations using experimental and theoretical computations [*Royer and Dieule-*
196 *saint, 2000*].

197 We increase the temporal resolution of the high-speed camera to record these events
198 in more details. In Figure 3, compared to the displacement magnitude given in Figure 2(a)
199 we increased the temporal resolution to 1000 frames per second (initially 125 fps). More-
200 over, to increase the spatial resolution of the images (and the resulting displacement maps)
201 we are focusing on sub-parts of the Hele-Shaw cell where most of the grain displacement
202 takes place. These settings allow us to follow the stick-slip events using the optical equip-
203 ment with higher spatial and temporal resolution. In Figure 3(b) we see the location of the
204 analyzed area in the cell (the channels are white, the granular porous medium is black, the
205 analyzed part of the medium is grey).

206 Figure 3(b) also shows us how this stick-slip event starts inside the zone being com-
207 pacted around 20 cm away from the tip of the channels with a decompacting zone behind,
208 and the pulse, pair of compacting zone and decompacting zone behind, travels backward
209 towards the fingertip (in a direction opposite to the grains direction) propagates towards
210 the tip of the channels. This is very similar to the phenomenon that we observed in Fig-
211 ure 2(a) where the source of the microseismic emission starts inside the porous medium
212 and progresses towards the channel tips (see the encircled zone). The first part of the sig-
213 nal is more sensitive to the start of the event than the whole slip event. Hence, they locate
214 the equivalent of the epicenter, which is typically ahead of the fingers, as illustrated in
215 Figure 3. Later on, the displacement gets distributed around most of the fingertips, and
216 ends up with the slip of the grains around the tips. The ESEH method is more sensitive

217 to observe this evolution than the conventional arrival-time-based seismic location meth-
218 ods since the arrival time of the event does not vary with time but the energy emitted per
219 second does. As the time window gets enlarged, the sensors are more and more sensitive
220 to signals coming from a larger and larger area, and the resulting location, which consid-
221 ers that the source is point-like in the methods, seems to come approximately from points
222 belonging to the mobile region, closer to the fingertips.

223 **6 Conclusion**

224 In this article, we show that the digital images and acoustic signals are very good
225 (and coherent) monitoring tools to detect and localize fracturing and channeling in a porous
226 medium. Different acoustic events having different natures (and locations) are investigated
227 optically and acoustically (see Supplementary Figures S5-27 for more events and corre-
228 sponding event recordings). The deformation magnitude maps obtained from digital im-
229 age correlation method are compared with the acoustic signal based source localization
230 results. The size of the time windows was set to extend freely so that the method would
231 give multiple results for a single event for a better comparison. Depending on the polar-
232 ization found on different sensors, it is possible to define the type of the source leading
233 acoustic emissions. Localization results seem to fit well with displacement map obtained
234 from the optical analysis techniques.

235 **Acknowledgments**

236 We would like to thank Alain Steyer and Miloud Talib for the technical support. This
237 project has received funding from the European Union's Seventh Framework Programme
238 for research under grant agreement no 316889 - FLOWTRANS, INSU ALEAS TelluS
239 program, the International Associate Laboratory France-Norway on Deformation Flow and
240 fracture of disordered Materials LIA D-FFRACT, from the Universities of Oslo and Stras-
241 bourg via a gjesteforsker program and an IDEX Espoirs award. Furthermore, this work
242 was partly supported by the Research Council of Norway through its Centres of Excel-
243 lence funding scheme, project number 262644 and grant 213462/F20. The experimental
244 dataset and the Matlab routines used in this study can be found on www.doi.org/10.5281/zenodo.1316548

245

246 **References**

- 247 Accutech (1994), *Accutech Pneumatic Fracturing Extraction and Hot Gas Injection, Phase*
 248 *One: Applications Analysis Report*, DIANE Publishing Company.
- 249 Aki, K., and P. G. Richards (2002), *Quantitative Seismology, 2nd Ed.*, University Science
 250 Books.
- 251 Allen, R. V. (1978), Automatic earthquake recognition and timing from single traces, *Bul-*
 252 *letin of the Seismological Society of America*, 68(5), 1521–1532.
- 253 Aochi, H., B. Poisson, R. Toussaint, and J. Schmittbuhl (2011), Induced seismicity along
 254 a fault due to fluid circulation: conception and application, in *Japan Geoscience Union*
 255 *Meeting 2011, May 2011, Makuhari, Chiba, Japan*.
- 256 Baer, M., and U. Kradolfer (1987), An automatic phase picker for local and teleseismic
 257 events, *Bulletin of the Seismological Society of America*, 77(4), 1437–1445.
- 258 Blaber, J., B. Adair, and A. Antoniou (2015), Ncorr: open-source 2d digital image correla-
 259 tion matlab software, *Experimental Mechanics*, 55(6), 1105–1122.
- 260 Brandstein, M., J. Adcock, and H. Silverman (1997), A closed-form location estimator for
 261 use with room environment microphone arrays, *Speech and Audio Processing, IEEE*,
 262 5(1), 45–50, doi:10.1109/89.554268.
- 263 Butterworth, S. (1930), On the theory of filter amplifiers, *Wireless Engineer*, 7(6), 536–
 264 541.
- 265 Candela, T., B. Wassing, J. Ter Heege, and L. Buijze (2018), How earthquakes are in-
 266 duced, *Science*, 360(6389), 598–600.
- 267 Charléty, J., N. Cuenot, L. Dorbath, C. Dorbath, H. Haessler, and F. M. (2007), Large
 268 earthquakes during hydraulic stimulations at the geothermal site of soultz-sous-forets,
 269 *International Journal of Rock Mechanics and Mining Sciences*, 44(8), 1091 – 1105, doi:
 270 <http://dx.doi.org/10.1016/j.ijrmms.2007.06.003>.
- 271 Chevalier, C., A. Lindner, M. Leroux, and E. Clément (2009), Morphodynamics during air
 272 injection into a confined granular suspension, *Journal of Non-Newtonian Fluid Mechan-*
 273 *ics*, 158(1), 63–72.
- 274 Christenson, B., A. Reyes, R. Young, A. Moebis, S. Sherburn, J. Cole-Baker, and K. Brit-
 275 ten (2010), Cyclic processes and factors leading to phreatic eruption events: Insights
 276 from the 25 september 2007 eruption through ruapehu crater lake, new zealand, *Journal*
 277 *of Volcanology and Geothermal Research*, 191(1-2), 15–32.

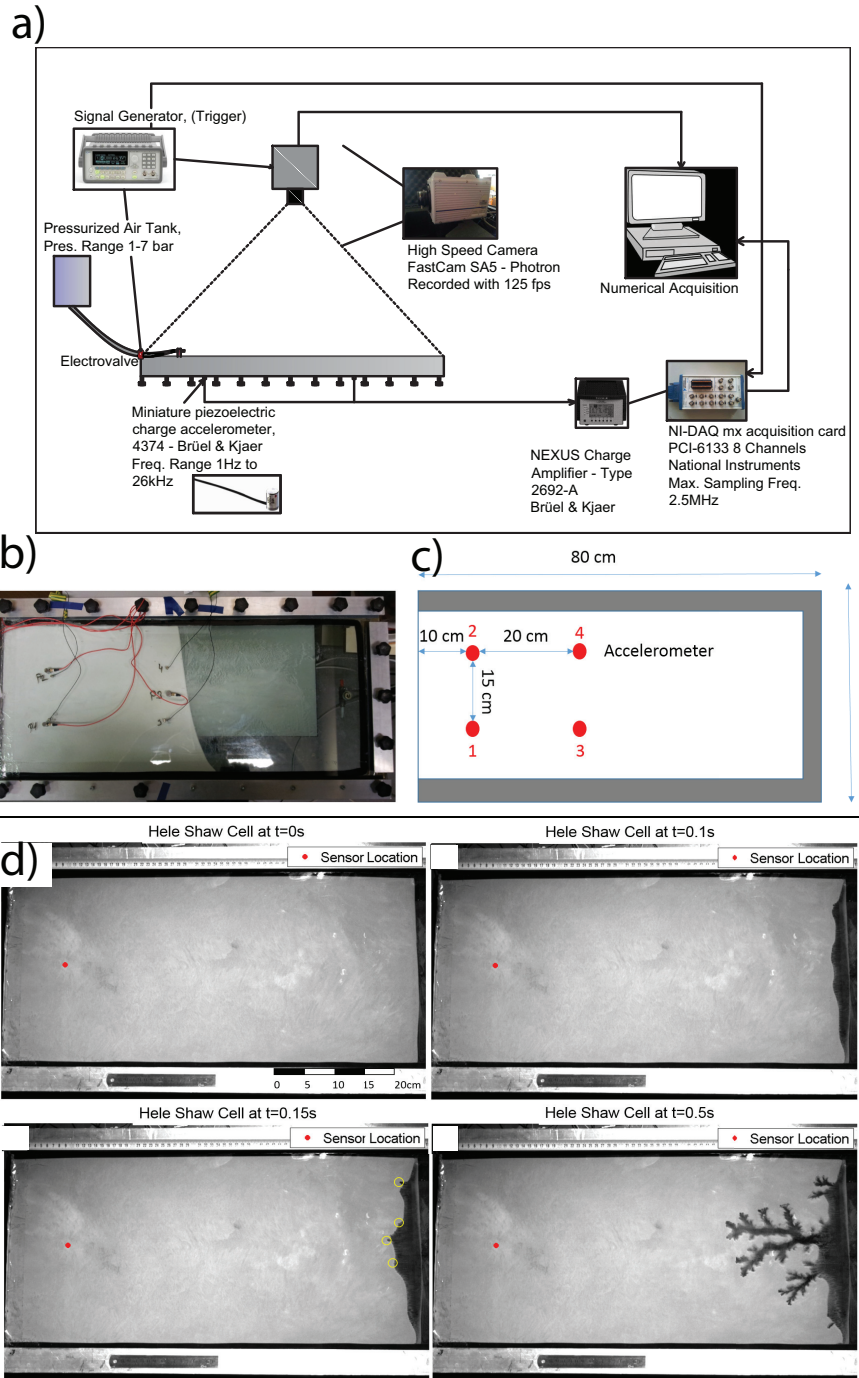
- 278 Cornet, F. (2015), *Elements of Crustal Geomechanics*, Cambridge University Press.
- 279 Cornet, F., J. Helm, H. Poitrenaud, and A. Etchecopar (1998), Seismic and aseismic slips
280 induced by large-scale fluid injections, in *Seismicity Associated with Mines, Reservoirs
281 and Fluid Injections*, pp. 563–583, Springer.
- 282 Cuenot, N., C. Dorbath, and L. Dorbath (2008), Analysis of the microseismicity induced
283 by fluid injections at the eggs site of soultz-sous-forets (alsace, france): Implications
284 for the characterization of the geothermal reservoir properties, *Pure and Applied Geo-
285 physics*, *165*(5), 797–828, doi:10.1007/s00024-008-0335-7.
- 286 Dorbath, L., N. Cuenot, A. Genter, and M. Frogneux (2009), Seismic response of the
287 fractured and faulted granite of soultz-sous-forets (france) to 5 km deep massive wa-
288 ter injections, *Geophysical Journal International*, *177*(2), 653–675, doi:10.1111/j.1365-
289 246X.2009.04030.x.
- 290 Earle, P. S., and P. M. Shearer (1994), Characterization of global seismograms using an
291 automatic-picking algorithm, *Bulletin of the Seismological Society of America*, *84*(2),
292 366–376.
- 293 Elnahrawy, E., X. Li, and R. Martin (2004), The limits of localization using signal
294 strength: a comparative study, in *Sensor and Ad Hoc Communications and Networks*,
295 *IEEE*, pp. 406–414, doi:10.1109/SAHCN.2004.1381942.
- 296 Eriksen, F. K., R. Toussaint, K. J. Måløy, and E. G. Flekkøy (2015), Invasion patterns
297 during two-phase flow in deformable porous media, *Frontiers in Physics*, *3*, 81.
- 298 Eriksen, F. K., R. Toussaint, A. L. Turquet, K. J. Måløy, and E. G. Flekkøy (2017a), Pres-
299 sure evolution and deformation of confined granular media during pneumatic fracturing
300 (in review), *Phys. Rev. E*.
- 301 Eriksen, F. K., R. Toussaint, A. L. Turquet, K. J. Måløy, and E. G. Flekkøy (2017b),
302 Pneumatic fractures in confined granular media, *Phys. Rev. E*, *95*, 062,901, doi:
303 10.1103/PhysRevE.95.062901.
- 304 Eriksen, F. K., R. Toussaint, A. L. Turquet, K. J. Måløy, and E. G. Flekkøy (2018), Pres-
305 sure evolution and deformation of confined granular media during pneumatic fracturing,
306 *Phys. Rev. E*, *97*, 012,908, doi:10.1103/PhysRevE.97.012908.
- 307 Farin, M., A. Mangeney, R. Toussaint, J. de Rosny, N. Shapiro, T. Dewez, C. Hibert,
308 C. Mathon, O. Sedan, and F. Berger (2015), Characterization of rockfalls from seismic
309 signal: insights from laboratory experiments, *JGR: Solid Earth*, *120*(10), 7102–7137.

- 310 Farin, M., A. Mangeney, J. De Rosny, R. Toussaint, J. Sainte-Marie, and N. Shapiro
 311 (2016), Experimental validation of theoretical methods to estimate the energy radiated
 312 by elastic waves during an impact, *Journal of Sound and Vibration*, 362, 176–202.
- 313 Fehler, M., L. House, and H. Kaieda (), Determining planes along which earth-
 314 quakes occur: Method and application to earthquakes accompanying hydraulic frac-
 315 turing, *Journal of Geophysical Research: Solid Earth*, 92(B9), 9407–9414, doi:
 316 10.1029/JB092iB09p09407.
- 317 Fink, M. (2015), Acoustic imaging with time reversal methods: From medicine to ndt,
 318 *AIP Conference Proceedings*, 1650(1), 13–23, doi:http://dx.doi.org/10.1063/1.4914591.
- 319 Gao, F., H. Xie, F. Zhou, Y. Ju, L. Xie, Y. Liu, Y. Gao, J. Liu, and R. Zhang (2014),
 320 Pneumatic fracturing method and system for exploiting shale gas, uS Patent App.
 321 14/335,935.
- 322 Garnier, J., and M. Fink (2015), Super-resolution in time-reversal focusing on a moving
 323 source, *Wave Motion*, 53, 80 – 93, doi:http://dx.doi.org/10.1016/j.wavemoti.2014.11.005.
- 324 Gershman, A., V. Turchin, and V. Zverev (1995), Experimental results of localization of
 325 moving underwater signal by adaptive beamforming, *Signal Processing, IEEE*, 43(10),
 326 2249–2257, doi:10.1109/78.469863.
- 327 Häring, M. O., U. Schanz, F. Ladner, and B. C. Dyer (2008), Characterisation of the basel
 328 1 enhanced geothermal system, *Geothermics*, 37(5), 469–495.
- 329 Hibert, C., A. Mangeney, G. Grandjean, and S. Nikolai (2011), Slope instabilities in
 330 Dolomieu crater, Réunion Island: From seismic signals to rockfall characteristics, *Jour-
 331 nal of Geophysical Research - earth surface*, 116, F04,032, doi:10.1029/2011JF002038.
- 332 Holland, A. A. (2013), Earthquakes triggered by hydraulic fracturing in south?central ok-
 333 lahomaearthquakes triggered by hydraulic fracturing in south?central oklahoma, *Bulletin
 334 of the Seismological Society of America*, 103(3), 1784, doi:10.1785/0120120109.
- 335 Jamtveit, B., Y. Ben-Zion, F. Renard, and H. Austrheim (2018), Earthquake-induced trans-
 336 formation of the lower crust, *Nature*, 556(7702), 487–491, doi:10.1038/s41586-018-
 337 0045-y.
- 338 Jolly, A., P. Jousset, J. Lyons, R. Carniel, N. Fournier, B. Fry, and C. Miller (2014),
 339 Seismo-acoustic evidence for an avalanche driven phreatic eruption through
 340 a beheaded hydrothermal system: An example from the 2012 tongariro erup-
 341 tion, *Journal of Volcanology and Geothermal Research*, 286, 331 – 347, doi:
 342 https://doi.org/10.1016/j.jvolgeores.2014.04.007.

- 343 Kobchenko, M., A. Hafver, E. Jettestuen, O. Galland, F. Renard, P. Meakin, B. Jamtveit,
344 and D. K. Dysthe (2013), Drainage fracture networks in elastic solids with internal fluid
345 generation, *EPL (Europhysics Letters)*, *102*(6), 66,002.
- 346 Malioutov, D., M. Cetin, and A. Willsky (2005), A sparse signal reconstruction perspec-
347 tive for source localization with sensor arrays, *Signal Processing, IEEE*, *53*(8), 3010–
348 3022, doi:10.1109/TSP.2005.850882.
- 349 Manga, M., and E. Brodsky (2006), Seismic triggering of eruptions in the far field: Volca-
350 noes and geysers, *Annu. Rev. Earth Planet. Sci.*, *34*, 263–291.
- 351 Niebling, M. J., E. G. Flekkøy, K. J. Måløy, and R. Toussaint (2010), Mixing of a granu-
352 lar layer falling through a fluid, *Physical Review E - Statistical, Nonlinear, and Soft Mat-
353 ter Physics*, *82*(1).
- 354 Oppenheimer, D. H. (1986), Extensional tectonics at the geysers geothermal area, califor-
355 nia, *Journal of Geophysical Research: Solid Earth*, *91*(B11), 11,463–11,476.
- 356 Peacock, M. (1996), Acoustic emission for detection of process-related damage in pressure
357 vessels and piping, pp. 2947 – 2947 – 9, doi:10.1117/12.259158.
- 358 Poland, M. P., A. Miklius, A. J. Sutton, and C. R. Thornber (2012), A mantle-driven surge
359 in magma supply to kīlauea volcano during 2003–2007, *Nature Geoscience*, *5*(4), 295.
- 360 Rivalta, E., and P. Segall (2007), Magma compressibility and the missing source for some
361 dike intrusions, *Geophysical Research Letters*, *35*(4), doi:10.1029/2007GL032521.
- 362 Royer, D., and E. Dieulesaint (2000), *Elastic Waves in Solids I: Free and Guided Propaga-
363 tion*, Advanced Texts in Physics, Springer.
- 364 Schuring, J., D. Kosson, C. Fitzgerald, and S. Venkatraman (1996), Pneumatic fractur-
365 ing and multicomponent injection enhancement of in situ bioremediation, uS Patent
366 5,560,737.
- 367 Stanchits, S., S. Mayr, S. Shapiro, and G. Dresen (2011), Fracturing of porous
368 rock induced by fluid injection, *Tectonophysics*, *503*(1), 129 – 145, doi:
369 <https://doi.org/10.1016/j.tecto.2010.09.022>, thermo-Hydro-Chemo-Mechanical Couplings
370 in Rock Physics and Rock Mechanics.
- 371 Sudo, Y., H. Ono, A. W. Hurst, T. Tsutsui, T. Mori, M. Nakaboh, Y. Matsumoto, M. Sako,
372 S. Yoshikawa, M. Tanaka, Y. Kobayashi, T. Hashimoto, T. Hoka, T. Yamada, H. Ma-
373 suda, and S. Kikuchi (1998), Seismic activity and ground deformation associated
374 with 1995 phreatic eruption of kuju volcano, kyushu, japan, *Journal of Volcanol-
375 ogy and Geothermal Research*, *81*(3), 245 – 267, doi:<https://doi.org/10.1016/S0377->

- 376 0273(98)00011-0.
- 377 Tazieff, H. (1989), Mechanisms of the nyos carbon dioxide disaster and of so-called
378 phreatic steam eruptions, *Journal of volcanology and geothermal research*, 39(2-3), 109–
379 116.
- 380 Terlizzi, J., and J. Minoo (2009), Multi-touch display screen with localized tactile feed-
381 back, uS Patent App. 12/069,352.
- 382 Travelletti, J., C. Delacourt, P. Allemand, J.-P. Malet, J. Schmittbuhl, R. Tous-
383 saint, and M. Bastard (2012), Correlation of multi-temporal ground-based op-
384 tical images for landslide monitoring: Application, potential and limitations,
385 *[ISPRS] Journal of Photogrammetry and Remote Sensing*, 70(0), 39 – 55, doi:
386 <http://dx.doi.org/10.1016/j.isprsjprs.2012.03.007>.
- 387 Trnkoczy, A. (1998), Understanding & setting sta/lta trigger algorithm parameters for the
388 k2, *Application Note*, 41, 16–20.
- 389 Turkaya, S., R. Toussaint, F. K. Eriksen, M. Zecevic, G. Daniel, E. G. Flekkøy, and K. J.
390 Måløy (2015), Bridging aero-fracture evolution with the characteristics of the acoustic
391 emissions in a porous medium, *Frontiers in Physics*, 3, 70.
- 392 Turkaya, S., R. Toussaint, F. K. Eriksen, O. Lengliné, G. Daniel, E. G. Flekkøy, and K. J.
393 Måløy (2016), Note: Localization based on estimated source energy homogeneity, *Re-
394 view of Scientific Instruments*, 87(9), 096,101.
- 395 Turquet, A., T. Bodin, P. Arroucau, M. Sylvander, and K. Manchuel (2018a), Quantifying
396 the seismic location uncertainties in french seismicity catalogues: Application to the
397 pyrenees (in prep), *Seismological Research Letters*.
- 398 Turquet, A. L., R. Toussaint, F. K. Eriksen, G. Daniel, D. Koehn, and E. G. Flekkøy
399 (2018b), Microseismic emissions during pneumatic fracturing: A numerical model to
400 explain the experiments, *Journal of Geophysical Research: Solid Earth*, 123(8), 6922–
401 6939, doi:10.1029/2017JB014613.
- 402 Valin, J., F. Michaud, J. Rouat, and D. Letourneau (2003), Robust sound source localiza-
403 tion using a microphone array on a mobile robot, in *IROS 2003. Proceedings. IEEE/RSJ*,
404 vol. 2, pp. 1228–1233 vol.2, doi:10.1109/IROS.2003.1248813.
- 405 Valkó, P., and M. Economides (1995), *Hydraulic fracture mechanics*, Wiley.
- 406 Wong, J., L. Han, J. Bancroft, and R. Stewart (2009), Automatic time-picking of first ar-
407 rivals on noisy microseismic data, *CSEG. 0 0.2 0.4 0.6 0.8, 1(1.2)*, 1–4.

408 Zhu, Q., S. Tannenbaum, and S. H. Kurtzman (2007), Optical tomography
409 with ultrasound localization for breast cancer diagnosis and treatment mon-
410 itoring, *Surgical Oncology Clinics of North America*, 16(2), 307 – 321, doi:
411 <http://dx.doi.org/10.1016/j.soc.2007.03.008>, pre and Postoperative Cancer Imag-
412 ing: Practical and Innovative Approaches.



112 **Figure 1.** (a) The acquisition chain of the aero-fracturing experiments with a Hele-Shaw cell. The signal
 113 acquisition card, camera and the electrovalve connected to the air pump are triggered at the same time via a
 114 TTL signal sent from the signal generator to have synchronized optical and acoustic data. The sensors are
 115 placed on the bottom glass plate of the Hele-Shaw cell using a solid crystallized phenyl salicylate. (b) The
 116 image showing the accelerometers stick under the Hele-Shaw cell is given. In (c), accelerometers are sketched
 117 and numbered. Red dots show the positions of the accelerometers. (d) We present several snapshots of the cell
 118 during injection.

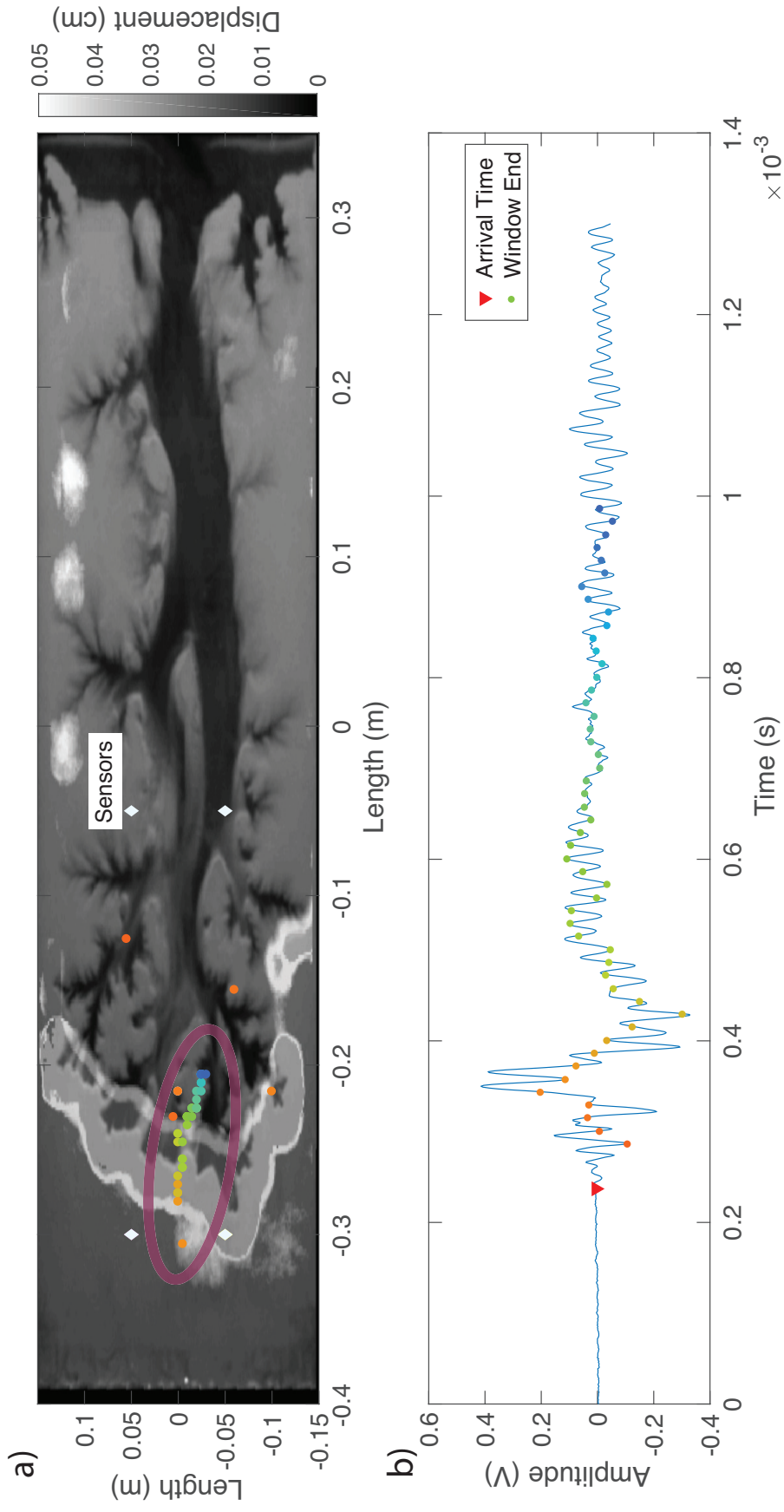


Figure 2. Localization of an acoustic event. (a): The localized source and receiver positions are indicated. Diamond markers show the accelerometer locations. The circle markers with different colors show the ESEH results with different input signal lengths starting from the red triangle at (b) and ending at the associated colored dot. The grayscale bar indicates the optically computed displacement magnitude in cm. (b): The acoustic event with different window sizes are presented. The red triangle shows the picked arrival time, which is the start of the signal for all time windows. The colored dots are the different ends of all windows used, resulting in different locations shown in (a).

Norm of bead displacement in successive 1 ms time windows (tw)

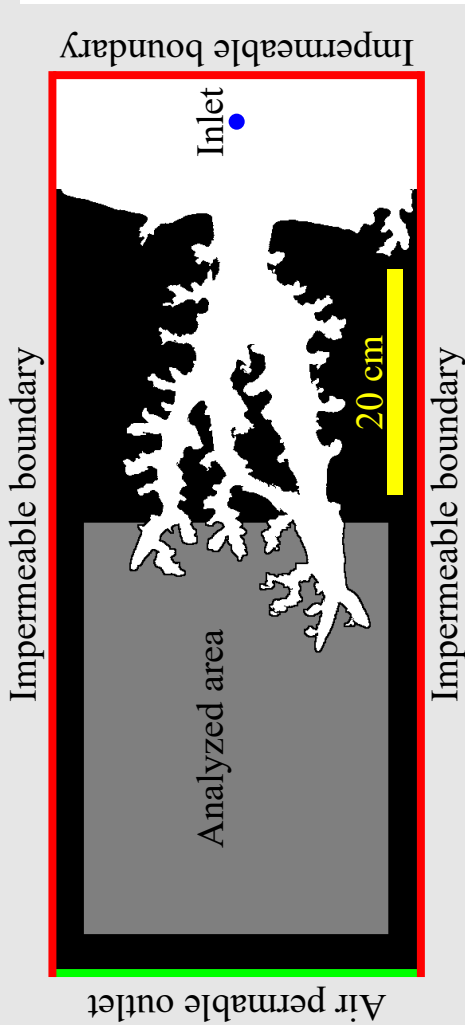
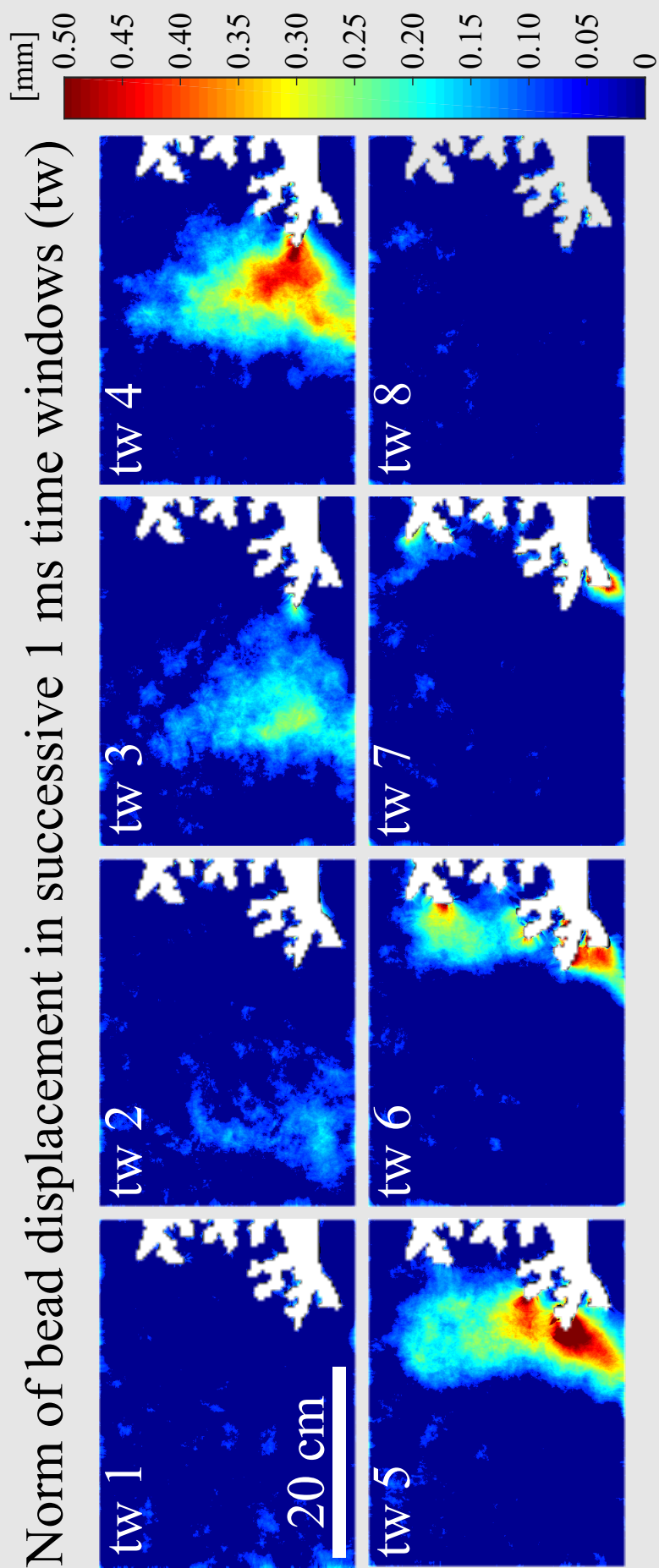


Figure 3. a) Displacement magnitude (mm) in successive time windows (tw). The image set covers 8 ms. b) Sketch of the Hele-Shaw cell and the location of the analyzed area.